NOTES

Polybaric partial melting in the continental mantle: Evidence from mantle xenoliths from Qilin, Guangdong Province

XU Yigang[1], YAN Wen[2], SUN Min[3], LIU Ying[1], HE Zaicheng[1] & SHI Lanbin[4]

1. Guangzhou Institute of Geochemistry, Chinese Academy of Sciences, Guangzhou 510640, China;
2. Institute of South China Oceanography, Chinese Academy of Sciences, Guangzhou 510240, China;
3. Department of Earth Sciences, The University of Hong Kong, China;
4. Institute of Geology, State Seismological Bureau, Beijing 100029, China

Abstract **The extremely low Ti content (160—245 μg/g) in clinopyroxene in some spinel peridotites from Qilin, South China is indicative of high degree of partial melting, inconsistent with their relatively high clinopyroxene modes (7.4%—12.4%). These clinopyroxenes show fractionated HREE patterns ($(Gd/Yb)_n$<0.2), suggesting the involvement of garnet in the melting regime. These REE patterns can be modeled as residues of 22%—23% fractional melting from a primitive mantle, first in garnet stability field (12%) then continuing in spinel stability field (10%—11%) after breakdown of garnet to pyroxenes and spinel. Such a polybaric melting suggests the lithospheric thinning and rapid mantle upwelling in south China during the Cenozoic. This is consistent with the dominant MORB-OIB isotopic signature and high thermal gradient of the lithospheric mantle in this region, and supports the contention that the formation of South China Sea basin is related to southward migration of continental lithosphere extension, rather than passive back-arc basin.**

Keywords: mantle xenoliths, trace element, polybaric melting, Qilin.

Modern igneous petrology[1] and theoretical modeling[2] suggest that basalts are not melting products of the mantle at a given depth, but likely represent the mixture of decompression melts of different degrees from a melting interval. In other words, mantle melting is a continuous polybaric fractional melting rather than equilibrium melting. Because heat transfers from the bottom to the top of decompressing mantle, melting starts from the deep garnet stability field and continues to the shallow spinel or plagioclase stability field. In the same tectonic context, the initial and final depths of the melting interval depend on the mantle potential temperature and lithospheric thickness[1, 2]. Mantle starts to melt at a great depth when the potential temperature is high and melting continues to a very shallow level if the lithosphere is sufficiently thin. The formation of many continental basaltic provinces is associated with lithospheric thinning[3]. This promotes further decompressional uplift of the asthenosphere.

Given the fact that the polybaric melting can explain fairly well the geochemical feature of basalts——the melting products of the mantle, information for this process is expected to be recorded in melting residues (i.e. peridotites). However, the evidence for this mechanism is still scarce[4, 5]. Abundant xenoliths have been recovered from the Cenozoic basalts in Qilin, Guangdong Province[6], and some of them show peculiar geochemical characteristics[7, 8] (i.e. fractionated HREE) that could have resulted from polybaric melting. In this note, we report new trace element data for the Qilin peridotites. These data and modeling results are used to constrain the melting mechanism and to shed light on the relationship between mantle processes and regional tectonic evolution.

1 Samples and analytical methods

The Qilin xenoliths contain spinel lherzolite (harzburgite), spinel and garnet pyroxenites, and minor granulite[6]. Spinel lherzolite and harzburgites are investigated in this study. Their typical mineral assemblage (table 1) is olivine (50%—68%), orthopyroxene (16%—38%), clinopyroxene (4.7%—17.6%) and spinel (1%—3.5%). The samples have coarse grained and prophyroclastic texture. The Qilin samples are serpentinized to various degrees. Thus, trace element analyses are largely concentrated on Cpx separates. Only a few whole rock powders have been analyzed for the purpose of comparison.

The analyses of trace element (REE, Ti, Zr, Nb, Ta, Hf, Rb, Sr, Ba, U, Th, Y) abundances were performed at the Guangzhou Institute of Geochemistry, CAS using an Inductively Coupled Plasma-Mass spectrometer (ICP-MS) PE 6000. The analytical procedure is similar to that described by Xu (2000). Precision for REE and HFSE is estimated to be 5%—10% from the international USGS reference sample BHVO-1 and internal standard RO-A1.

2 Results

Trace element compositions of Cpx separates and some whole rocks are listed in table 1. Two types of chondrite-normalized REE patterns can be distinguished. The first type is characterized by a flat HREE distribution ($(Ho/Yb)_n$=0.91—1.07) and variable LREE ($(La/Yb)_n$ =0.4—10.5). The variation from LREE-depleted to LREE-enriched pattern can be ascribed to chromatographic metasomatism[12]. A concave downward REE pattern($(Gd/Yb)_n$>1.2)is noted for QLS-18 and a flat REE pattern for QLS-16. These two samples are characterized by conspicuously high Ti (Zr and Hf) contents compared to other samples (table 1). The second type is the V-shaped REE pattern at Eu $(Gd/Yb)_n$=0.1—0.2). Similar REE characteristics have been observed for the Qilin peridotites which were analyzed in a different laboratory[8]. Therefore, the HREE fractionation cannot be the analytical artifact. For a given sample, Cpx and bulk rocks show similar REE patterns (fig. 1(a)). This suggests that the

Table 1 Modal composition (%) and trace element abundance (μg/g) of Qilin peridotite xenoliths

	GPQ-3	GPQ-3*	QLS-5	QLS-9	QLS-15	GPQ-1	GPQ-1*	QLS-3	QLS-16	QLS-18	QLS-21	QLS-22	QLS-23
Ol	62.0		66.1	50.8	59.3			63.5	63.5	63.3	51.9	65.8	63.3
Opx	22.8		18.8	38.7	29.6			19.5	26.0	24	37.1	25.7	15.6
Cpx	12.4		11.7	7.4	8.3			13.8	8.9	10.2	9.3	7.5	17.6
Sp	2.7		3.4	3.1	2.4			3.1	1.7	2.5	1.7	1.0	3.5
Mg#ol	0.907		0.903	0.901	0.905			0.898	0.903	0.898	0.890	0.914	0.899
Cr#sp	0.20		0.22	0.14	0.22			0.17	0.20	0.23	0.13	0.43	0.24
Sc	62.5	9.9	73.8	70.8	87.3	46.7	12.3	69.1	58.1	72.9	62.8	83.4	63.2
Ti	160	40	245	176	189	808	326	1642	4158	3527	2077	536	865
Th	0.19	0.02	0.19	0.23	0.22	0.38	0.11	0.08	0.75	0.52	0.59	0.44	0.38
U	0.05	0.01	0.05	0.05	0.05	0.11	0.04	0.02	0.16	0.16	0.07	0.11	0.10
Hf	0.06	0.01	0.11	0.04	0.03	0.18	0.06	0.52	0.78	1.72	0.65	0.29	0.23
Ta	0.02	0.00	0.03	0.03	0.03	0.03	0.03	0.03	0.02	0.05	0.06	0.15	0.05
Rb	0.70	0.83	0.68	0.90	0.96	0.34	0.93	0.50	0.79	0.94	0.84	1.01	1.05
Sr	24.0	49.00	41.4	38.4	48.4	21.0	5.46	80.2	39.0	110.6	79.9	76.5	35.9
Y	3.93	0.42	4.85	4.26	4.39	9.89	1.43	13.49	9.44	11.69	17.72	3.63	9.37
Zr	1.68	0.23	5.94	1.63	1.75	3.84	2.13	15.99	20.40	45.91	20.33	18.40	7.84
Nb	0.15	0.05	0.16	0.19	0.17	0.35	0.48	0.24	0.13	0.21	0.45	0.71	0.68
Ba	0.50	0.90	0.82	0.60	0.63	1.48	2.02	0.40	0.82	0.83	2.67	3.00	13.17
La	1.08	0.12	1.20	1.60	1.67	0.63	0.42	3.69	2.24	3.07	3.92	5.19	1.31
Ce	1.53	0.17	2.32	2.31	2.57	1.21	0.75	9.15	5.29	8.80	10.91	11.19	2.76
Pr	0.13	0.02	0.27	0.17	0.22	0.18	0.09	1.15	0.75	1.51	1.43	1.28	0.34
Nd	0.40	0.05	1.04	0.49	0.63	0.94	0.38	4.77	3.65	7.77	5.99	5.07	1.56
Sm	0.08	0.01	0.21	0.08	0.10	0.40	0.09	1.20	1.13	2.14	1.62	1.01	0.50
Eu	0.03	0.01	0.06	0.03	0.03	0.17	0.04	0.45	0.39	0.67	0.58	0.28	0.20
Gd	0.18	0.02	0.31	0.18	0.19	0.78	0.16	1.78	1.56	2.32	2.40	0.98	0.91
Tb	0.05	0.01	0.07	0.05	0.05	0.19	0.03	0.33	0.28	0.39	0.46	0.14	0.20
Dy	0.46	0.05	0.59	0.49	0.50	1.50	0.23	2.07	1.64	2.13	2.88	0.69	1.40
Ho	0.13	0.02	0.16	0.14	0.15	0.36	0.06	0.46	0.34	0.42	0.62	0.13	0.33
Er	0.47	0.06	0.56	0.51	0.53	1.20	0.18	1.35	0.95	1.16	1.77	0.36	0.98
Tm	0.09	0.01	0.10	0.09	0.10	0.17	0.03	0.22	0.15	0.18	0.27	0.05	0.16
Yb	0.59	0.09	0.68	0.64	0.67	1.18	0.19	1.32	0.88	1.07	1.62	0.34	0.98
Lu	0.11	0.02	0.13	0.12	0.12	0.16	0.03	0.23	0.15	0.19	0.27	0.06	0.17

Columns with * are whole rock analyses, others are analyses of clinopyroxenes. Modes are determined by point-counting (>2000 points) under a microscope.

REE composition of Cpx represents that of whole rock and is not affected by subsolidus equilibrium between coexisting minerals.

3 Peculiar compositional feature of the Qilin peridotites

Peridotite xenoliths from Wangqing, Jilin Province display compositional variations which are similar to those of peridotites from worldwide localities[13]. Thus they can be used as representative of the "normal" mantle. Cpx in the Samoan peridotites exhibit extremely strong fractionation in HREE that may have resulted from large degree of polybaric melting[4]. The peculiar composition of the Qilin samples is revealed by comparison with these references (fig. 2).

(1) In the plot of Ti in Cpx against $Cr\#_{sp}$, most Qilin samples follow the partial melting trend, whereas two samples (QLS-18 and QLS-16) are plotted above this general trend (fig. 2(a)) due to the conspicuously high Ti contents. The convex-upward REE pattern of QLS-18 suggests the equilibrium with LREE-enriched silicate melts. Thus, the high Ti contents in these Cpx likely resulted from mantle metasomatism. In contrast, some samples (GPQ-3, QLS-5, 9, 15) are plotted below the partial melting trend because of their extremely low TiO_2 at moderate $Cr\#_{sp}$ (0.14—0.22). Such characteristics cannot be reconciled with metasomatism. Ti contents in these Cpx vary between 160—245 μg/g, considerably lower than that in Cpx in the primitive mantle (>3000 μg/g)[10]. This is indicative of high degrees of partial melting. In fact, similar low Ti contents are only observed in harzburgites[8,13]. However, the Qilin samples with low Ti contents are lherzolites which contain 7.4%—12.4 % Cpx (table 1). Cpx in peridotite xenoliths from eastern China with equivalent Cpx contents are less depleted in Ti than the Qilin samples [8, 13]. Thus, trace element composition of some Qilin peridotites is not consistent with modal composition.

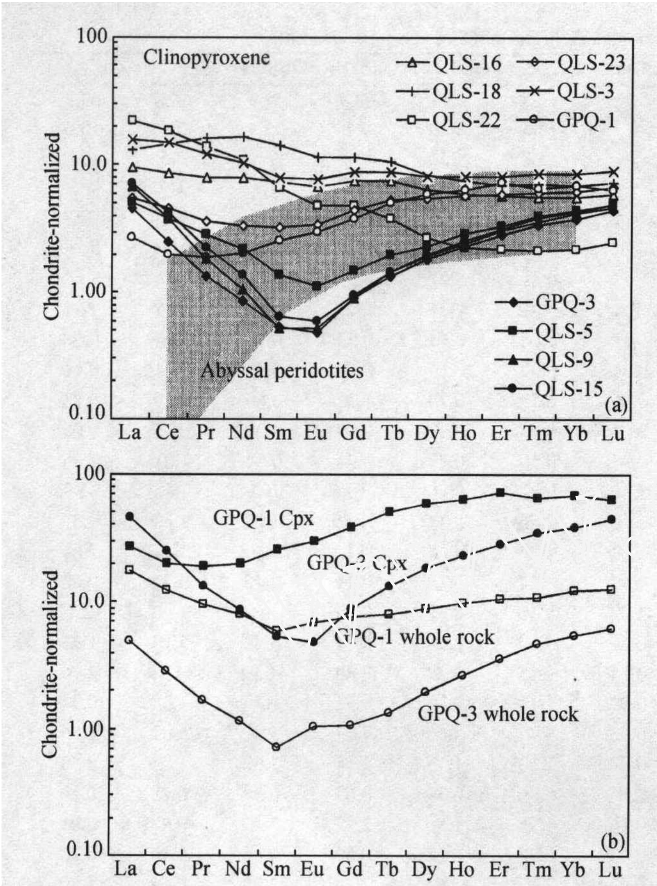

Fig. 1. REE abundances in peridotite xenoliths from Qilin. (a) Clinopyroxene; (b) comparison of REE abundance in whole rock and clinopyroxene. Data of abyssal peridotites and chondrite normalizing data are from refs. [10, 11].

(2) The negative correlation between Cpx and Opx modes in the Qilin peridotites is opposite to what expected for mantle melting in the spinel stability field (fig. 2(b)).

(3) Cpx with low Ti contents show fractionated HREE. The Gd/Yb ratio of these Cpx is less than 0.5, significantly lower than the ratios (about 1.2) of common spinel peridotites. These samples fall within the field of the Samoan peridotites (fig. 2(c)).

4 Melting mechanism of the upper mantle beneath Qilin

In order to study the melting mechanism and have a quantitative estimation on the extent of partial melting, we have used the fractional melting model[10] to calculate moderately incompatible element compositions of clinopyroxenes in the residues as a function of melting degree. Fig. 3 shows the results of this modeling based on Y and Yb contents in Cpx in the spinel stability field, compared with measured Y and Yb contents in the Qilin samples. It is noted that the peridotites from Wangqing closely follow the melting trend, suggesting that the melting of the upper mantle beneath Wangqing took place in the spinel stability field. Good match between modeled trend and measured values is also noted for some Qilin samples. However, the samples with low Ti contents are plotted above the modeled trend due to their relatively high Yb content at given Y content. This indicates that the REE composition in these samples cannot be fully explained by a fractional melting within the spinel stability field.

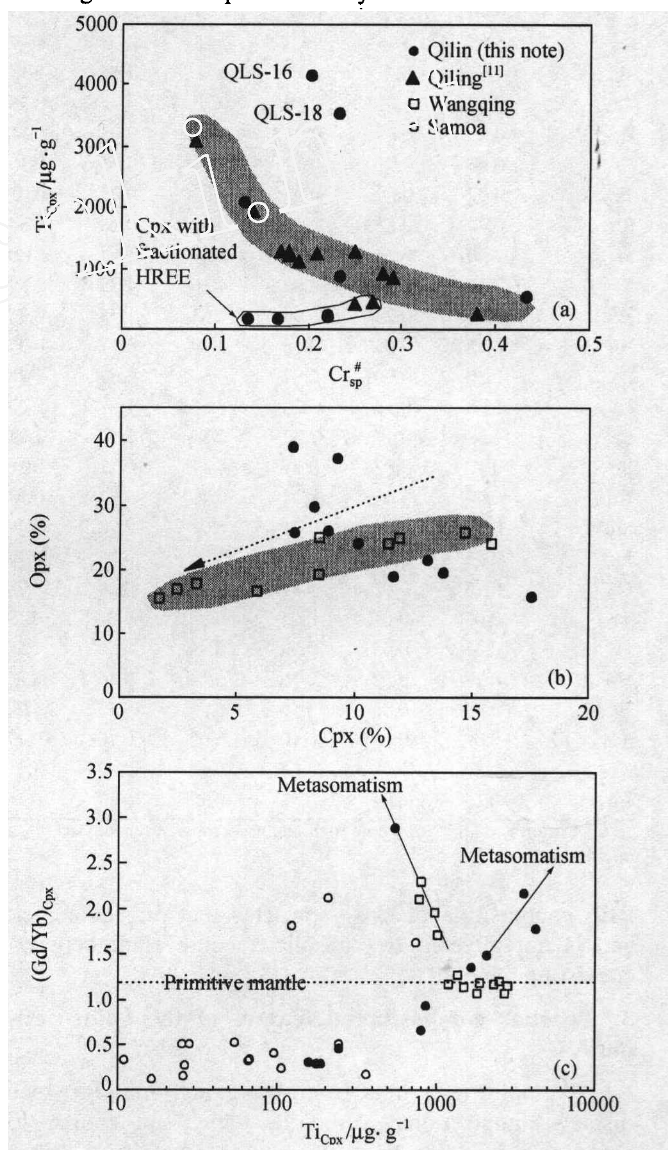

Fig. 2. (a) Ti in Cpx versus Cr$\#_{sp}$; (b) Cpx mode versus Opx mode; (c) $(Gd/Yb)_{cpx}$ versus Ti in Cpx. The shaded field is the composition range of the Wangqing peridotites that represent the partial melting trend [13]. The dashed line indicates the melting trend of abyssal peridotites[13]. Data of the Samoan xenoliths are from ref. [4].

Following differences are noted for partition coefficients of trace elements between Cpx-melt and garnet-melt[14]: (i) $D^{gt/melt}$ of HREE are fractionated, whereas $D^{cpx/melt}$ of HREE remain almost constant; (ii) on an extended trace element diagram, $D^{gt/melt}$ show negative

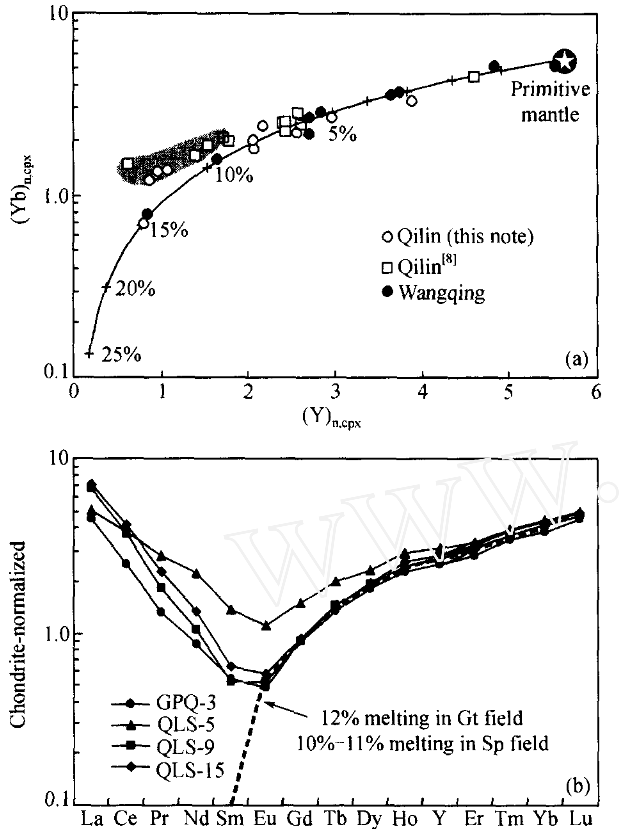

Fig. 3. (a) Comparison of Y and Yb contents of clinopyroxenes in the Qilin peridotite xenoliths with the calculated melting trend using fractional melting model within spinel stability field. Note the deviation of the Qilin samples with low Y contents from the melting trend. The fractional melting model and REE partition coefficients are after [10, 14]. The trace element composition in primitive cpx is calculated from primitive mantle composition assuming modal composition as the following: 55% ol, 18% cpx, 25% opx and 2% sp. (b) Comparison between the modeled results of polybaric fractional melting and the trace element compositions of Qilin xenolihs. The cpx composition of sample GPQ-3 can be nicely fitted by 12% melting in stability field of garnet lherzolite, breaking down to pyroxene and spinel, and then continuing melting of 11% in the stability of spinel lherzolite. The starting materials are Ol, 55%; Opx, 20%; Cpx, 15%; Gt, 10%; melting reaction in garnet field[15]: Ol, 3%; Opx, 3%; Cpx,70%; Gt, 24%; melting reaction in spinel field[16]: Ol, -6%; Opx, 28%; Cpx, 67%; Sp, 11%; decompression reaction of garnet is after [10]: 0.17 Ol + Gt → 0.53 Opx + 0.47 Cpx + 0.17 Sp.

anomalies in Y, Sr and Ti and positive Zr anomaly relative to adjacent REE, whereas $D^{cpx/melt}$ show negative anomalies in Zr and Ti and no anomaly for other elements[14]. Therefore, fractionated HREE, positive Zr and negative Y and Sr anomalies in Cpx are diagnostic of the former existence of a precursor garnet. Based on the fractionated HREE pattern and positive Zr anomaly in cpx, Hauri and Hart[4] proposed a polybaric partial melting (first in garnet stability field then continuing in spinel field) for the Samoan mantle. For the Qilin samples that deviate from the melting trend in the spinel field, their Zr contents have been affected by mantle metasomatism and thus cannot be used for garnet identification. Nevertheless, the compositions of the elements (Ti, HREE) unaffected by metasomatism are similar to those in the Somoan Cpx (fig. 2(c)), strongly indicating the involvement of garnet in the melting of the Qilin upper mantle.

We thus propose that the Qilin peridotites represent the residues of polybaric partial melting. To test this inference, we performed calculation using the fractional melting model[10] to monitor the REE variation during the polybaric melting. The calculation was done in three successive steps. The melting starts in the stability field of garnet lherzolite, followed by the breaking down of garnet into Cpx and Opx and then by the continuing melting in the spinel stability field. While the amount of melting in the garnet field is adjusted to simulate the observed degree of HREE fractionation, the absolute concentrations of the HREE are dependent on the degree of melting in the spinel field. Fig. 3(b) compares the modeling results with the REE patterns of Cpx in the Qilin peridotites. The Cpx composition of sample GPQ-3 (QLS-9, 15 as well) can be nicely fitted by 12% melting in stability field of garnet lherzolite and then continuing melting of 10%—11% in the spinel stability after breaking down of garnet to pyroxene and spinel. The total degree of melting amounts to 22%—23%.

The polybaric melting model can explain the discrepancy between relatively high Cpx modes (7.4%—12.4%) and the high degree of partial melting as suggested by very low Ti contents in Cpx, because of the formation of additional Cpx by garnet break-down. On the other hand, the consumption of Cpx (>70%) is more important than that of Opx (<3%) in the melting regime of garnet stability field[16]. This may be the reason of the negative correlation between Cpx and Opx modes in the Qilin samples. Spinel formed owing to garnet break-down would inherit the low Cr# of the former garnet. This results in deviation of the samples that experienced polybaric melting from the common partial melting trend.

The modeling calculation also reveals that the visible HREE fractionation requires relatively extensive partial melting (>20%) and melting in the garnet field is not less than 8%. These may partly account for the scarcity of visible HREE fractionation in the spinel peridotites, and the absence of HREE fractionation would not necessarily preclude the polybaric melting history in a given region.

5 Implications of polybaric melting for deep processes

The degree of partial melting estimated for the Samoan xenoliths is as high as 42%. More than half of this melting is required to take place in the garnet stability field. Such an important melting in garnet field may be accomplished in an environment with high rate of mantle upwelling and high potential temperature of the mantle[4]. The polybaric melting has also been documented in abyssal peridotites[10] and continental mantle xenoliths[5]. In the case of the abyssal peridotites, the polybaric melting is only recognized in samples recovered from fracture zone near hot spot[10]. It is also important to note that the Rhon samples are from a region where mantle upwelling (diapirism) is well-established[5]. It thus follows that the hot mantle temperature may be a pre-requisite of polybaric melting, especially for producing the recognizable trace element signature. This is a reasonable inference because the high potential temperature of mantle would ensure the intersection of thermal gradient and mantle solidus at a great depth and a high total degree of partial melting as well. The trace element composition of some Qilin xenoliths requires about 12% melting to occur in the garnet field. By inference, this may reflect the relatively high temperature of the mantle beneath south China, in agreement with the high thermal gradient derived from the Qilin garnet websterites[17].

The thickness of the lithosphere beneath south China varies between 70—80 km. The identification of initial melting in garnet field suggests that the Qilin xenoliths may have originated in the asthenosphere or at the base of the lithosphere, if spinel-garnet transition is assumed at a depth of 70—80 km for the region of high thermal gradient[2]. The lithosphere origin can be precluded because the heat supplied by conduction from the asthenosphere is not sufficient for as high as 23% of the anhydrous melting of the lithospheric mantle[2]. Moreover, the high rate of mantle upwelling as suggested by the polybaric melting mechanism cannot be reconciled with the passive uplift of the lithosphere due to asthenospheric upwelling. We thus speculate that the Qilin mantle was asthenospheric at the time of melting, and it converted to the lithosphere due to the subsequent thermal relaxation. A likely scenario is that the asthenosphere rose in the form of diapirism from the garnet stability field and finally reequlibrated in spinel stability field. Later, this part of the mantle was affected by metasomatism.

The high rate of mantle upwelling and lithospheric thinning as suggested by polybaric melting mechanism is consistent with the results of other independent studies in south China. (i) Enriched lithospheric sources were involved in the early Tertiary basalts in SE China, whereas OIB-type asthenosphere sources were associated with the late Tertiary to recent basalts[18-19]. Such a temporal shift in magma source can be ascribed to lithospheric thinning throughout time. During the early Cenozoic, the lithosphere was relatively thick and prevented melting of the asthenosphere. Magmas were mainly derived from fusible components in the lithosphere because volatile can considerably lower the solidus of peridotites. The asthenosphere began to melt since the Miocene when the lithosphere became sufficiently thinned. (ii) Sr-Nd isotopic compositions of mantle-derived xenoliths reveal that the shallow mantle beneath south China is isotopically similar to MORB and OIB, probably as a result of replacement of old lithosphere by asthenosphere[20]. Therefore, xenolith data support the contention that the formation of South China Sea basin is related to southward migration of lithosphere extension, rather than passive back-arc basin.

Acknowledgements This work was supported by the National Natural Science Foundation of China (Grant Nos. 49925308 and 49733110), the Ministry of Science and Technology of China (pre-selected 39 project) and the Chinese Academy of Sciences (Grant Nos. KZ951-B1-406-04 and KZCX2-209).

References

1. Klein, E. M., Langmuir, C. H., Global correlation of ocean ridge basalt chemistry with axial depth and crustal thickness, J. Geophy. Res., 1987, 92: 8089.
2. McKenzie, D. P., Bickle, M. J., The volume and composition of melt generated by extension of the lithosphere, J. Petrol., 1988, 29: 625.
3. White, R. S., McKenzie, D. P., Mantle plume and continental flood basalts, J. Geophys. Res., 1995, 100: 17543.
4. Hauri, E. H., Hart, S. R., Constraints on the melt migration from mantle plumes: a trace element study of peridotite xenoliths from Savai'i, Western Samoa, J. Geophys. Res., 1994, 99: 24301.
5. Witt-Eickschen, G. E., Kramm, U., Mantle upwelling and metasomatism beneath Central Europe: Geochemical and isotopic constraints from Mantle xenoliths from the Rhon (Germany), J. Petrol., 1997, 38: 479.
6. Xu, X., O'Reilly, S. Y., Zhou, X. et al., A xenolith-derived geotherm and the crust-mantle boundary at Qilin, southeastern China, Lithos., 1996, 38: 41.
7. Xu, Y. G., The trace element signature of the mantle-derived xenoliths from Qilin, Guangdong province and its geological significance, Guangdong Geology (in Chinese), 1998, 13: 39.
8. Xu, X., O'Reilly, S. Y., Griffin, W. L. et al., Genesis of young lithospheric mantle in southeastern China: an LAM-ICPMS trace element study, J. Petrol., 2000, 41: 111.
9. Xu, Y. G., Distribution of trace elements in spinel and garnet peridotites, Science in China, Series D, 2000, 43: 166.
10. Johnson, K. T. M., Dick, H. J. B., Shimizu, N., Melting in the oceanic upper mantle: An ion microprobe study of diopsides in abyssal peridotites, J. Geophy. Res., 1990, 95: 2661.
11. Sun, S. S., McDonough, W. F., Chemical and isotopic systematics of oceanic basalts: implications for mantle composition and processes, Magmatism in the Ocean Basins (eds. Saunders, A. D., Norry, M. J.), London: Geological Society Special Publication, 1989. 313—345.
12. Navon, O., Stolper E. Geochemical consequence of melt percolation: the upper mantle as a chromatographic column, J. Geol., 1987, 95: 285.
13. Xu, Y. G., Menzies, M. A., Vroon, P. et al., Texture-temperature-Geochemistry relationship in the upper mantle as revealed from spinel peridotite xenoliths from Wangqing, NE China, J. Petrol., 1998, 39: 469.
14. Johnson, K. T. M., Experimental determination of partition coefficients for rare earth and high-field-strength elements between clinopyroxene, garnet and basaltic melt at high pressures, Contrib. Mineral. Petrol., 1998, 133: 60.
15. Kinzler, R. J., Melting of mantle peridotite at pressure approaching the spinel to garnet transition: application to mid-ocean ridge petrogenesis, J. Geophys. Res., 1997, 102: 853.
16. Walter, M. J., Melting of garnet peridotite and the origin of komatiitic and depleted lithosphere, J. Petrol., 1998, 39: 29.
17. Xu, Y. G., Lin, C. Y., Shi, L. B., The geotherm of the lithosphere beneath Qilin, SE China: A re-appraisal and implications for P-T estimation of Fe-rich pyroxenites, Lithos., 1999, 47: 181.
18. Zou, H. P., Li, P. L., Rao, C. T., Geochemistry of Cenozoic volcanic rocks in ZhuJiangkou Basin and its geodynamic significance. Geochimica (in Chinese), 1995, 18(suppl): 33.
19. Chung, S. L., Cheng, H., Jahn, B. M. et al., Major and trace element, Sr-Nd isotope constraints on the origin of Paleogene volcanism in South China prior to the South China Sea opening, Lithos., 1997, 40: 203.
20. Fan, W. M., Menzies, M. A., Yin, H. H. et al., The nature and process of the deep lithosphere beneath southeast China, Geotectinica et Metallogenia (in Chinese), 1993, 17: 23.

(Received March 23, 2001)